Schweizerischer Erdbebendienst
Service Sismologique Suisse
Servizio Sismico Svizzero
Swiss Seismological Service

ETH zürich

SITE CHARACTERIZATION REPORT

SLCF: La Chaux-de-Fonds (NE) - Aéroport des Eplatures

Clotaire Michel, Manuel Hobiger, Donat Fäh

Last Modification: 8th June, 2017

Schweizerischer Erdbebendienst (SED)
Service Sismologique Suisse
Servizio Sismico Svizzero
Servizi da Terratrembels Svizzer

ETH Zurich
Sonneggstrasse 5
8092 Zurich
Schweiz
clotaire@sed.ethz.ch

Contents

Summary

The new station SLCF was installed in the Les Eplatures Airport in La Chaux-de-Fonds (NE) and the installation site has been characterized. We performed passive seismic array measurements that successfully allowed us to retrieve 1D velocity profiles at the station site. The site shows 35 m of unconsolidated sediments with velocities from 180 to 520 m/s. A clear contrast with the rock at 1600 m/s is present at 35 m depth.
$V_{s,30}$ is 405 m/s and the site corresponds to ground type B in the Eurocode 8 (CEN, 2004) and type C in the SIA261 (SIA, 2014). The theoretical 1D SH transfer function computed from the inverted profiles shows a large peak at about 4 Hz reaching an amplification factor of 4.5 and matches well the observed amplification at the station.

1 Introduction

In the framework of the second phase of the Swiss Strong Motion Network (SSMNet) renewal project, a new installation in the Les Eplatures Airport in La Chaux-de-Fonds (NE), close to the meteorological station was decided. It is located in the Swiss Jura, in the elongated depression filled by loam on which the city has been built (see Fig. 1). The new station went operational on 20 September 2016.

Figure 1: Overview of the landscape close to station SLCF, including one station of the array measurement (LCF502). Station SLCF is located behind the cemetery, at the head of the train.

2 Geological setting

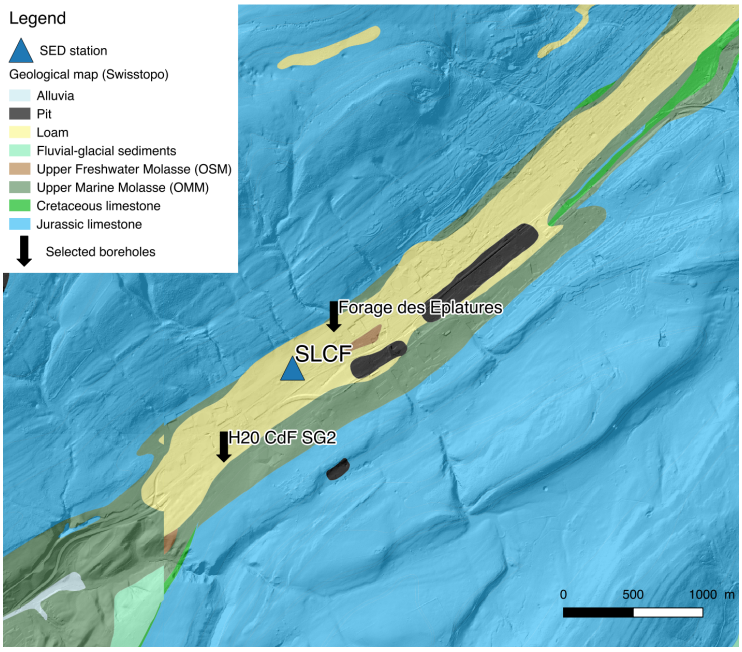

Figure 2: Geological map of the area of La Chaux-de-Fonds superimposed on a relief map (data: © 2017 swisstopo JD100042).

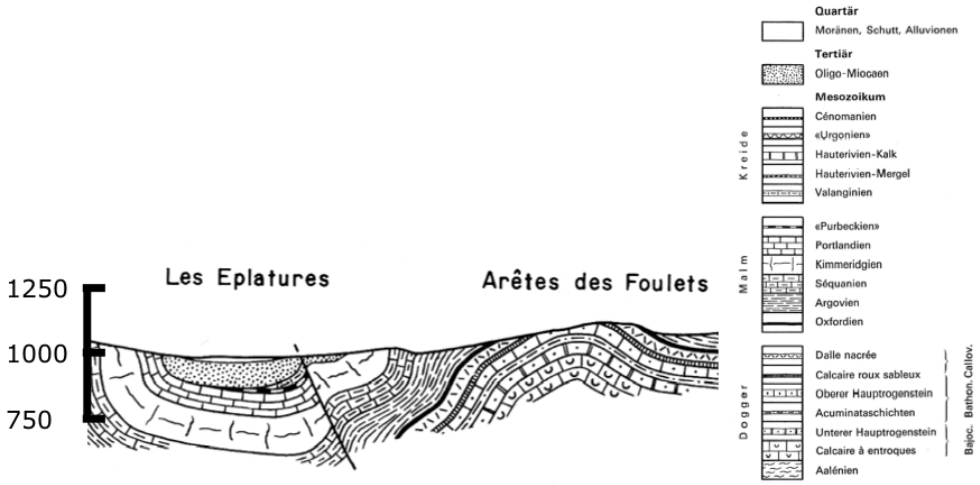

Figure 3: Geological NW-SE cross section through the SLCF (Les Eplatures) site based on the note of the local geological map (© 2017 swisstopo JD100042).

La Chaux-de-Fonds, as well as the close town of Le Locle, is located in the Swiss Jura, in an elongated depression (syncline of the Mesozoic layers) parallel to the mountain range filled by Tertiary sedimentary rocks and Quaternary sediments (Fig. 2 and Fig. 3). The upper part of these sediments is a shallow layer of loam or peat (less than 25 m according to Fig. 3). The depression is mostly filled by the underlying Miocene rock (about 100 m thickness in the centre): marls and limestone from the Upper Freshwater Molasse (OSM, Tortonian age) overlaying marls and sandstones of the Upper Marine Molasse (OMM,

Langhian-Serravallian age). The bedrock is made of the massive Mesozoic (Jurassic) limestone of lower Tithonian age that can be seen outcropping at the sides of the depression. The log of a deep borehole (Forage des Eplatures, see Fig. 2) of 348 m depth performed in 1964 was provided by the Canton, although its coordinates are probably imprecise. It is located 250 m NE from point LCF501 of the ambient vibration array and 450 m from the permanent station. It indicates 10.5 m of unconsolidated sediments (clay) over 12 m of Tertiary OSM conglomerates, sitting on the Mesozoic limestone bedrock (Tithonian age). One can notice an interface with marls at 315 m depth. Another borehole (H20 CdF SG2), much shallower, in the centre of the depression, 750 m SW from the SLCF station, shows more than 15 m of unconsolidated sediments (loam).
On the federal website `map.geo.admin.ch`, the site has been classified as ground type E (SIA261) where loam was present, F1 on the peat and A when Tertiary or Mesozoic rock was outcropping.

3 Site characterization using passive measurements

3.1 Measurements and data set

We investigated the local underground structure by passive seismic array measurements, which took place on December 7th, 2016. The layout of the seismic array is shown in Fig. 4.
The parameters of the array are given in Table 1. For this measurement, 12 Nanometrics Centaur dataloggers named NR42 to NR49 and NR52 to NR55 and 16 Lennartz 3C 5 s seismometers were available. Each datalogger can record on the two ports A (channels EH1, EH2, EH3 for Z, N, E directions) and B (channels EH4, EH5, EH6 for Z, N, E directions). Time synchronization is ensured by GPS. The sensors were placed on metal tripods. For better coupling with the ground, the tripods were placed in 10 cm deep holes, when possible.
The sensor coordinates were measured using a differential GPS device (Leica Viva GS10), including only a rover station and using the Real Time Kinematic technique provided by Swisstopo (swipos). It allowed an absolute positioning with an accuracy better than 2 cm on the Swissgrid.

Table 1: Characteristics of the seismic array measurements in La Chaux-de-Fonds.

Array name	Number of sensors	Minimum interstation distance [m]	Aperture [m]	Recording time [min]
LCF	16	8	500	167

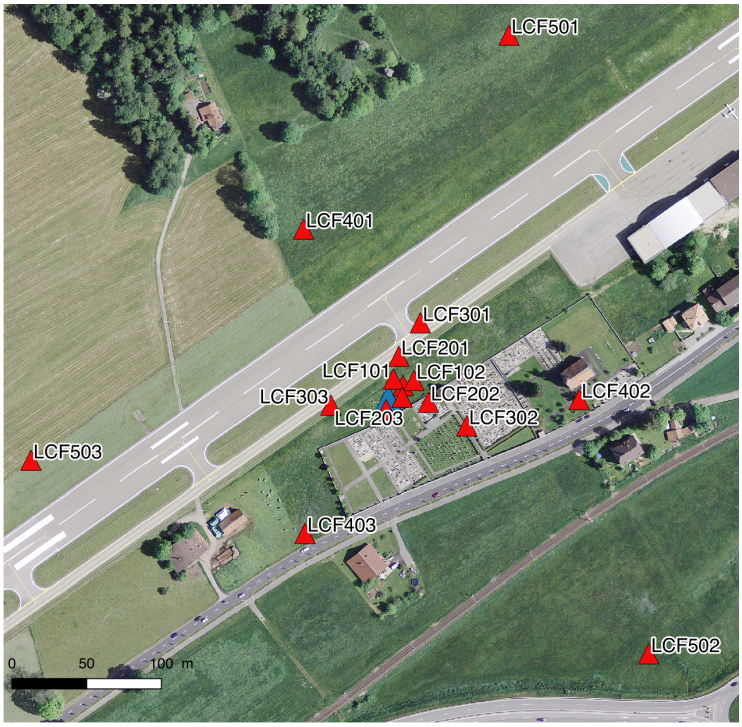

Figure 4: Layout of the array measurements at site SLCF. Array stations are in red and SLCF station in blue.

The largest time windows were extracted, for which all the sensors of the array were correctly placed and the GPS synchronization was ensured. While the recordings are well correlated below 1 Hz, strong differences are noted for higher frequencies. Only few harmonic disturbances can be noted. Tilt can be noted at point LCF403 as well as a strong peak at 20 Hz in the three components.
Orientations of the sensors were checked by maximizing the correlation with the central station at low frequencies (Poggi et al., 2012b). Corrections lower than 8 ° were performed.

3.2 Single station measurement results

3.2.1 H/V curves

The H/V curves across the array are presented in Fig. 5. A first peak at 0.73 Hz is present, that can also be seen on all single station measurements performed in La Chaux-de-Fonds, including those located on Mesozoic rock (Fig. 6). It can be assumed that this resonance corresponds to a deep interface, within the rock. The observed variations are most probably related to picking uncertainty and not to actual variations in this layer, considering the wavelength it corresponds to.
A second peak is present through the array except at points LCF501 and LCF503 that can be considered to be located on rock, despite the geological map (Fig. 7). In the central part of the array, close to the station, the second peak frequency equals 3.5 Hz. The situation is smoothly changing towards the edges of the depression. This peak corresponds to loose deposits, thicker in the centre of the depression and shallower at the edges. It should be noticed that the peaks are not always clear to be picked and some expert judgment had to be used. At some points, a third peak at frequencies higher than 10 Hz corresponds to a surficial layer.
In the city, the second peak can also be observed (Fig. 8), with high values at the edges of the depression, lower values in the centre, and is consistently absent on Mesozoic rock. The four points located most to the North-East in the depression (LCF15-16-18-19 in the database) show however a different pattern. The second peak, very clear, occurs at frequencies as low as 0.95 Hz and the fundamental is hard to see and maybe even absent.

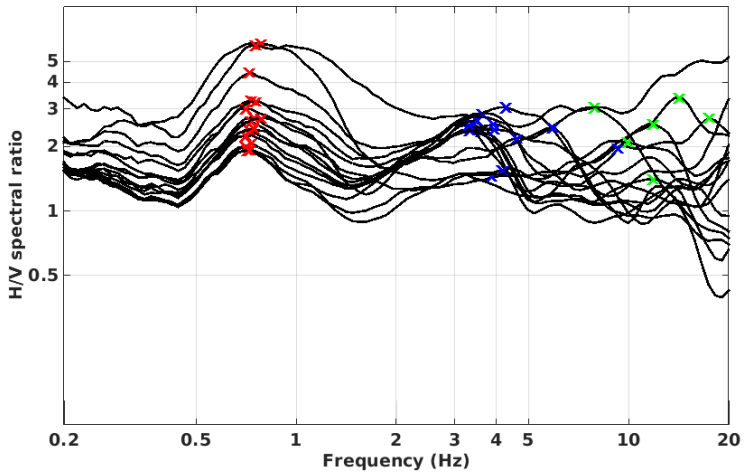

Figure 5: Comparison of H/V spectral ratios (time-frequency analysis code V. Poggi) between the different points of the arrays.

All the methods to compute H/V ratios are compared at point LCF000 in Fig. 9, in which the classical methods were divided by $\sqrt{2}$ to correct for the Love waves contribution (Fäh et al., 2001). The 3C FK analysis (Capon method) computed from rings 1 and 2 only matches well with the H/V analysis (see section 3.3). In terms of amplitude, all these methods match well.
WaveDec has only be used for the whole array (see section 3.4) and does not show comparable results (not displayed here).

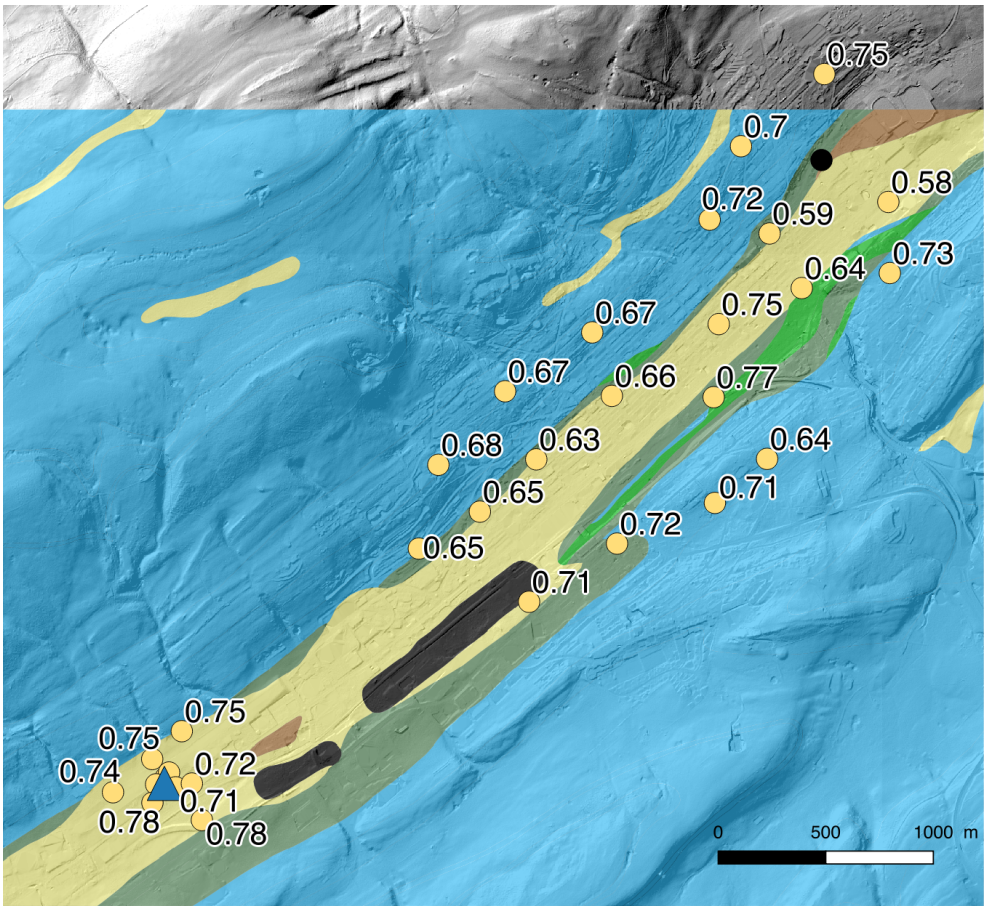

Figure 6: Map of the identified fundamental peaks in the H/V ratios (frequency values in Hz) superimposed on the simplified geological map of the area (see Fig. 2 for the legend). Black dots indicate no value.

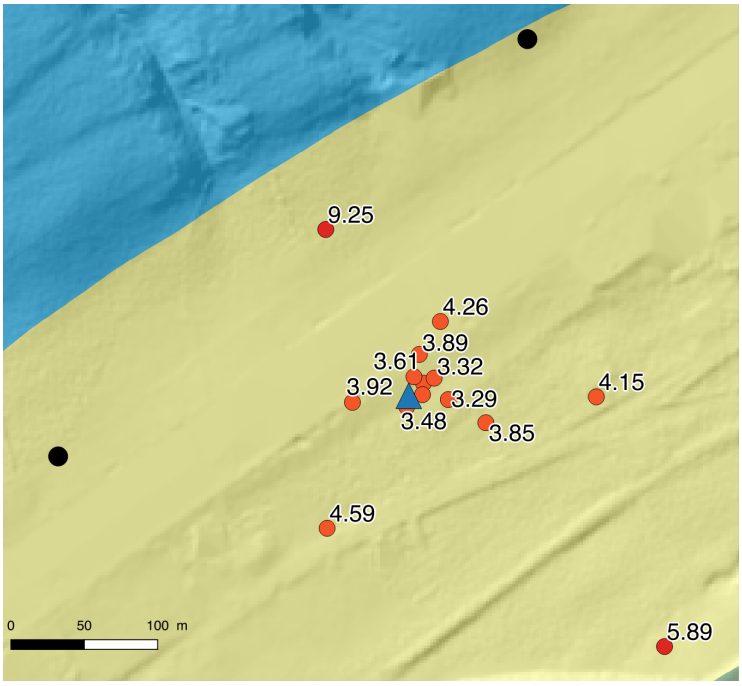

Figure 7: Map of the identified second peaks in the H/V ratios (frequency values in Hz) superimposed on the simplified geological map of the area (see Fig. 2 for the legend). Black dots indicate no value (rock).

The fundamental peak at the SLCF station is therefore at 0.73 Hz, with a peak amplitude around 2 and the second peak at 3.5 Hz with a peak amplitude of 2.5.

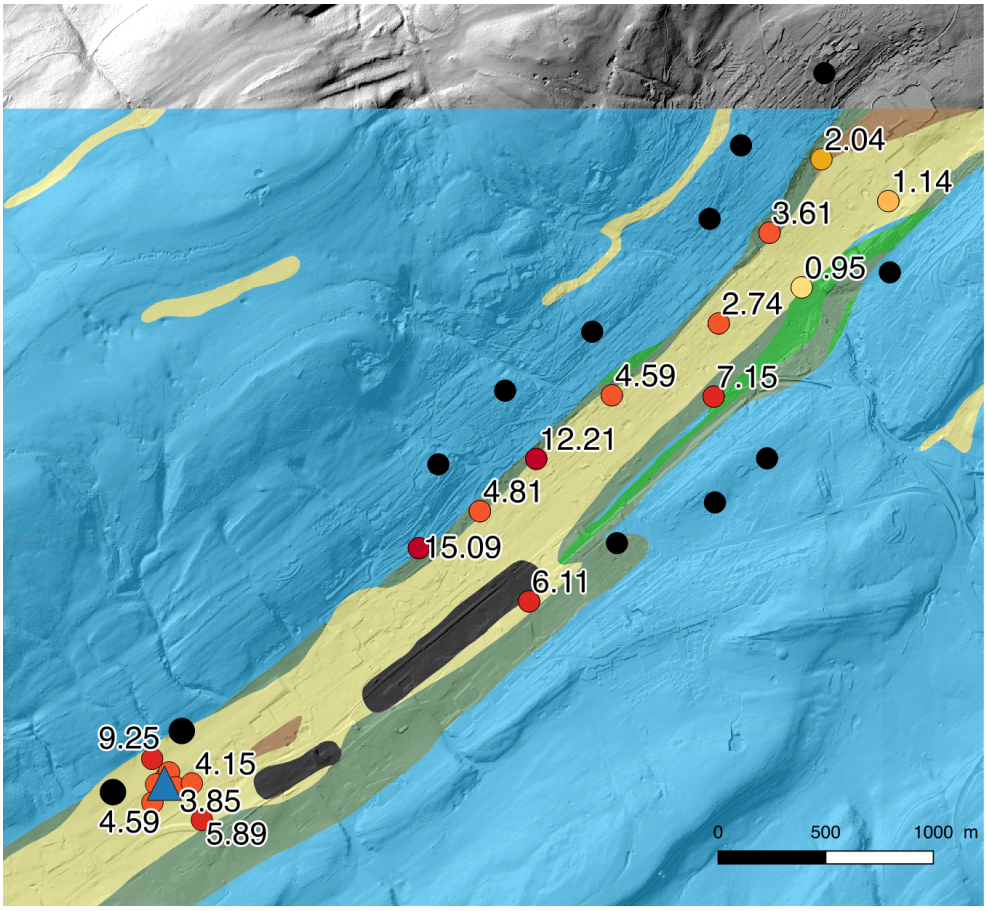

Figure 8: Map of the identified second peaks in the H/V ratios (frequency values in Hz) for the whole city superimposed on the simplified geological map of the area (see Fig. 2 for the legend). Black dots indicate no value (rock).

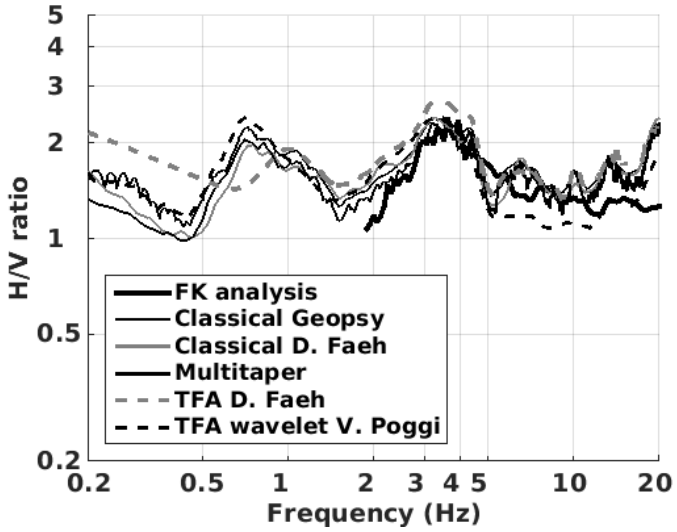

Figure 9: H/V spectral ratios for point LCF000 using the different codes. Classical methods were divided by $\sqrt{2}$.

3.2.2 Polarization analysis

Polarization analysis on the array data was performed to check for 2D resonance using the method of Burjánek et al. (2010). The wavefield does not show any particularly elliptical motion in the direction of the axis of the depression (Fig. 10). Therefore, 2D resonance can be excluded at this site.

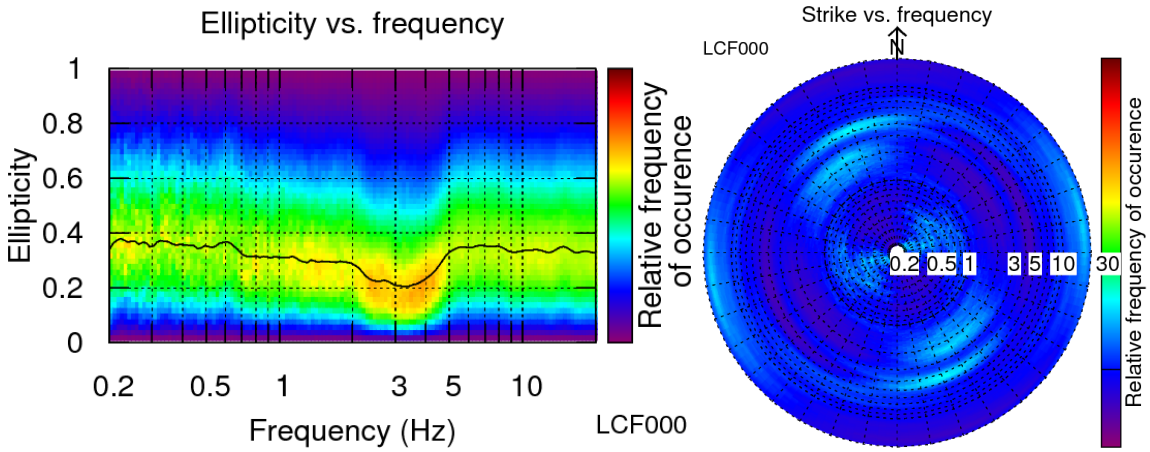

Figure 10: Polarization analysis at point LCF000. Left: Ellipticity (A trough in the ellipticity corresponds to polarized motion). Right: Strike of the polarization.

3.3 1- and 3-component high-resolution FK

Since the H/V analysis showed strong lateral variations below the array, several sub-arrays including gradually the rings, from the smallest to the largest, have been first analysed using the 1C high-resolution FK method implemented in the Geopsy software in order to avoid misinterpretation (Fig. 11). This shows the presence of what seems to be two osculation points at 4.6 and 9 Hz (and probably another one at 18 Hz). These features cause apparent increase in the velocity, actually due to the energy leaking between the fundamental and the first higher modes. The fundamental and small chunks of the higher modes could be picked. Only the smallest sub-array analysis provides a clear picture above 10 Hz while the others are blurred due to the lateral variations. Each sub-array contributes to a portion of the curve that is only slightly affected by shifts from one picking to another. The results of the 3-component HRFK analysis (Poggi and Fäh, 2010) for three sub-arrays are shown in Fig. 12, Fig. 13 and Fig. 14. Rayleigh waves modes from the 1C analysis are confirmed, while the second higher mode can be picked in addition. The mode addressing was performed using information from the inversion. Similarly as for Rayleigh waves, Love waves can be picked by chunks for each of the sub-arrays.

The ellipticity curve determined with the 3-component HRFK analysis matches the H/V ratios when using rings 1 and 2 only (Fig. 9 and Fig. 14). However, 3C analyses using larger arrays show a flat ellipticity due to the heterogeneities (Fig. 12 and Fig. 13).

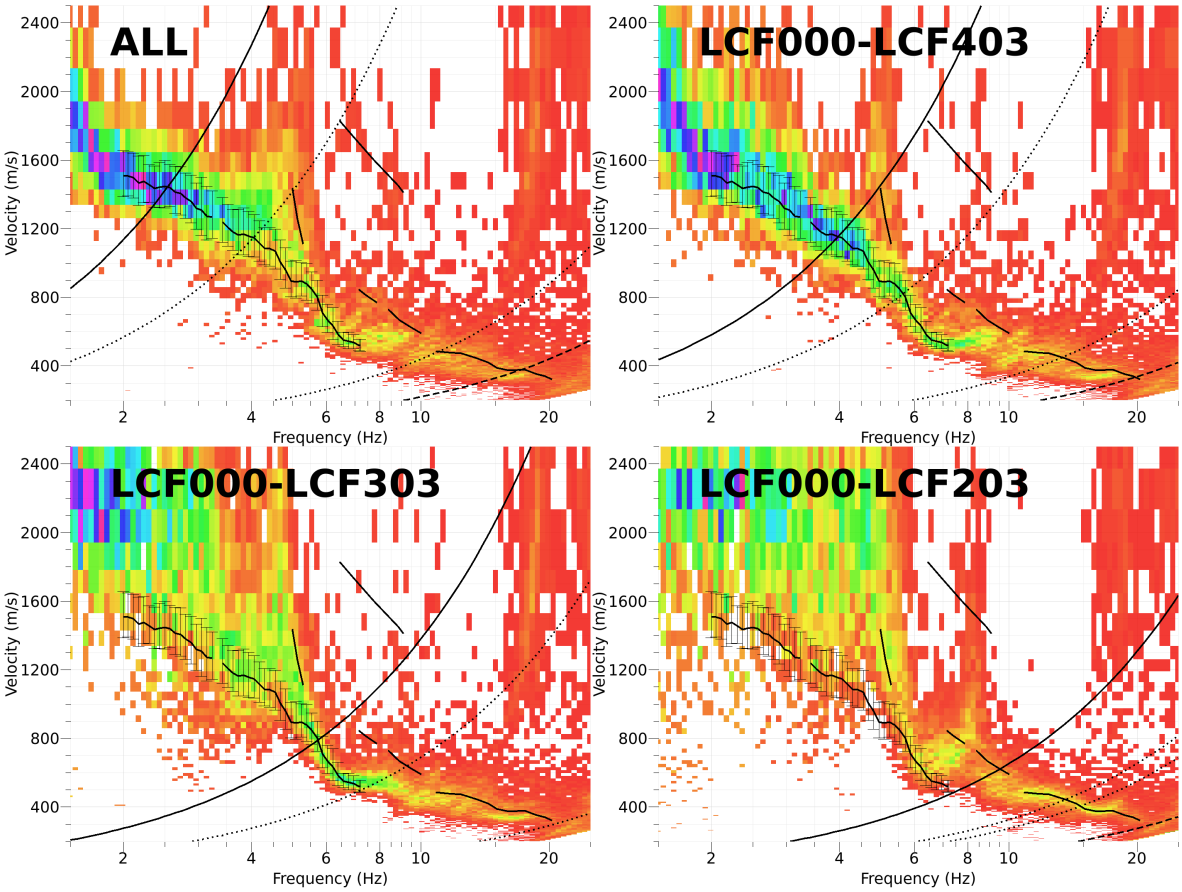

Figure 11: Dispersion curves obtained from the 1C HRFK analyses with different sub-arrays. The picking is based on the 1C and 3C analysis (see also Fig. 12, Fig. 13 and Fig. 14).

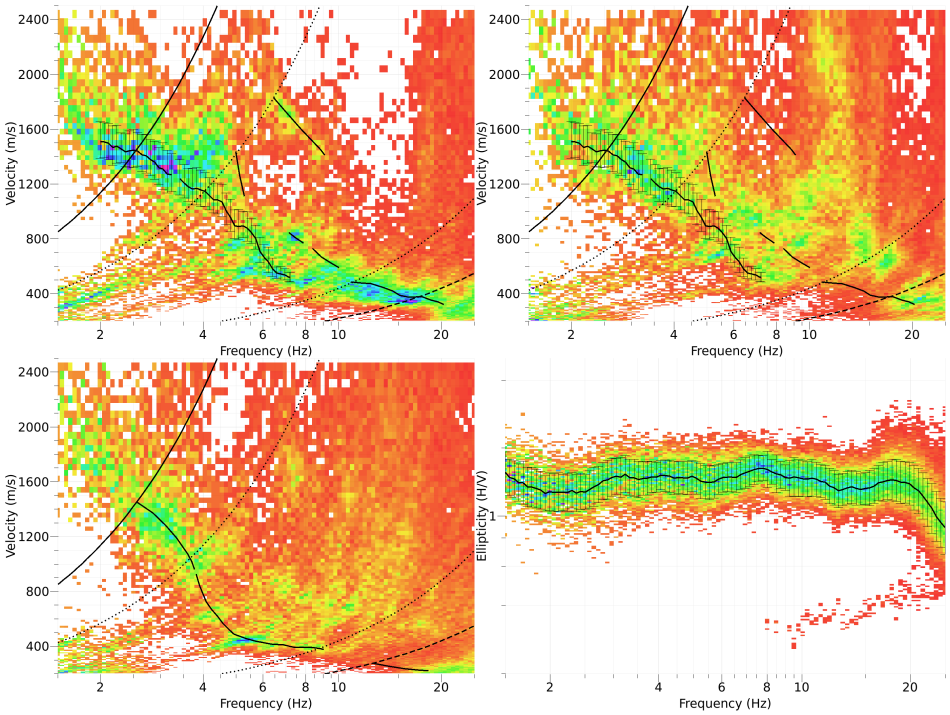

Figure 12: Dispersion curves obtained from the 3C HRFK analyses of the whole array. Top row: Vertical and radial component; bottom row: transverse component and ellipticity. The picking is based on the 1C and 3C analysis (see also Fig. 11, Fig. 13 and Fig. 14).

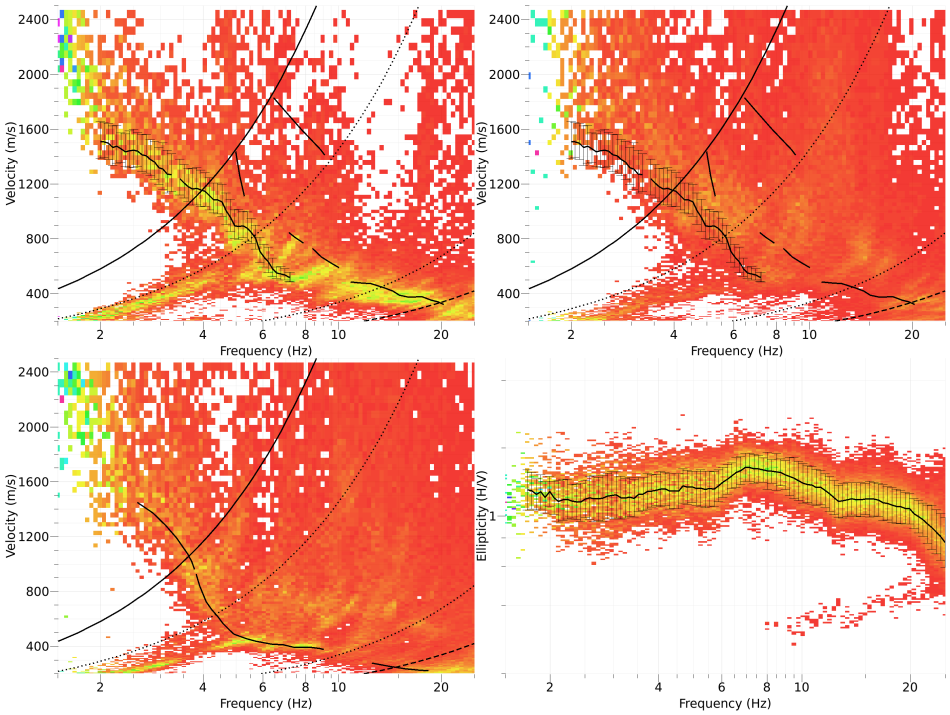

Figure 13: Dispersion curves obtained from the 3C HRFK analyses for the sub-array made of points LCF000 to LCF403. Top row: Vertical and radial component; bottom row: transverse component and ellipticity. The picking is based on the 1C and 3C analysis (see also Fig. 11, Fig. 12 and Fig. 14).

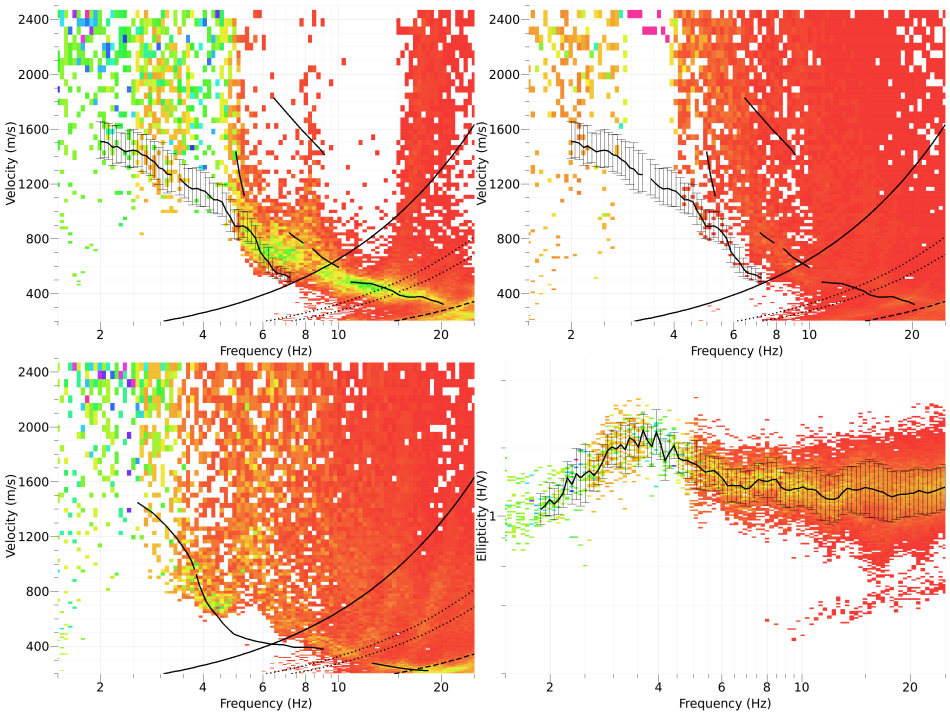

Figure 14: Dispersion curves obtained from the 3C HRFK analyses for the sub-array made of points LCF000 to LCF203. Top row: Vertical and radial component; bottom row: transverse component and ellipticity. The picking is based on the 1C and 3C analysis (see also Fig. 11, Fig. 12 and Fig. 13).

3.4 Wavedec

WaveDec (Maranò et al., 2012) has also been used to process the whole array data. This technique estimates the properties of multiple waves simultaneously with a maximum likelihood approach in the time domain. It was applied assuming the presence of 3 waves (Love and Rayleigh) with a γ value of 0.2 that penalises less the complexity and therefore may contain more noise.
The fundamental Love and Rayleigh wave dispersion curves, as well as the first higher Rayleigh wave mode, could be picked within the array limits (Fig. 15) and are compared to the FK analysis in section 3.5. The mode assignment was performed in the light of the results of the 3C FK analysis. The ellipticity of Rayleigh waves (Fig. 16) shows retrograde waves going close to the singularity between 2.9 and 3.7 Hz, which would correspond to the fundamental peak. However, the change of sense of rotation from prograde to retrograde, is probably an artefact. Lateral variations prevent from comparing to the single station analysis. The first higher mode of Rayleigh waves is prograde between 6.5 and 10 Hz where it could be picked (Fig. 17).

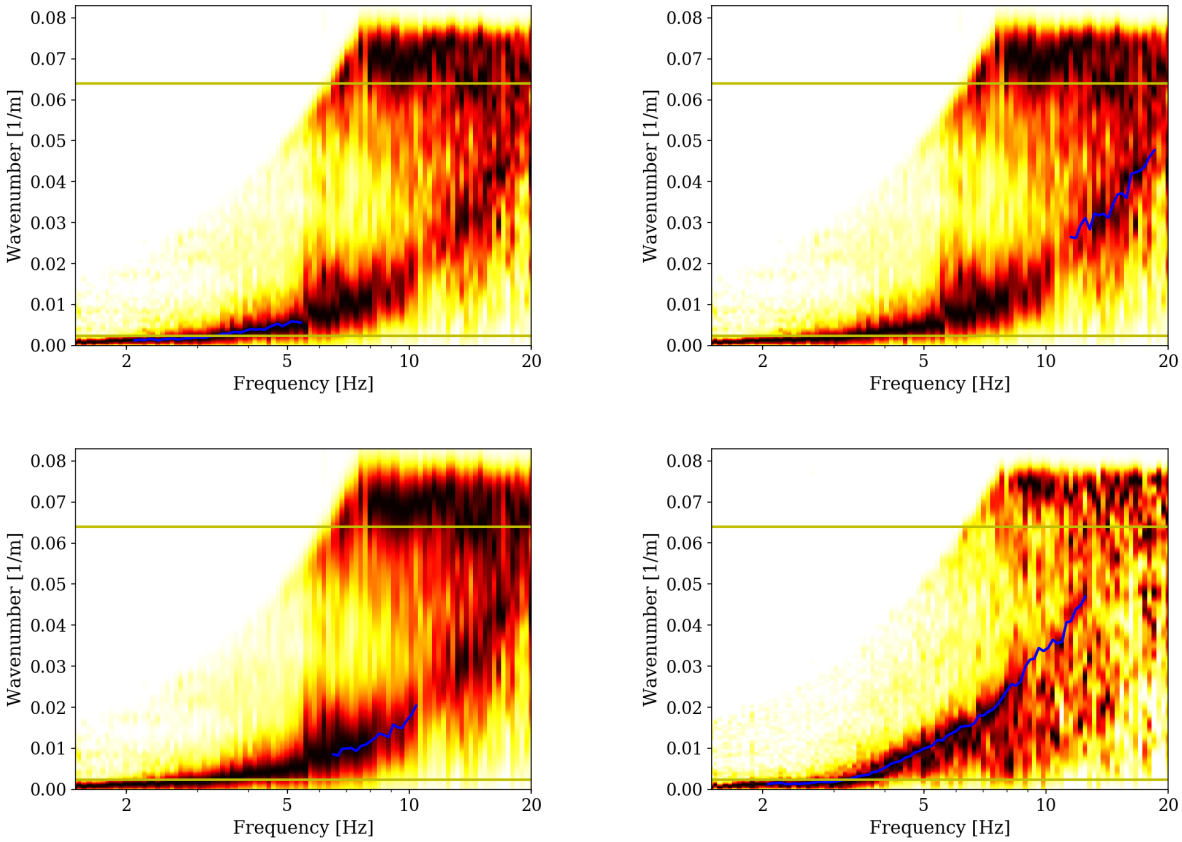

Figure 15: Rayleigh and Love wave dispersion curves obtained with the WaveDec technique (Maranò et al., 2012). Picked fundamental (top) and first higher (bottom left) modes of Rayleigh waves and fundamental mode (bottom right) of Love waves are shown. The yellow lines indicate the theoretical array resolution limits.

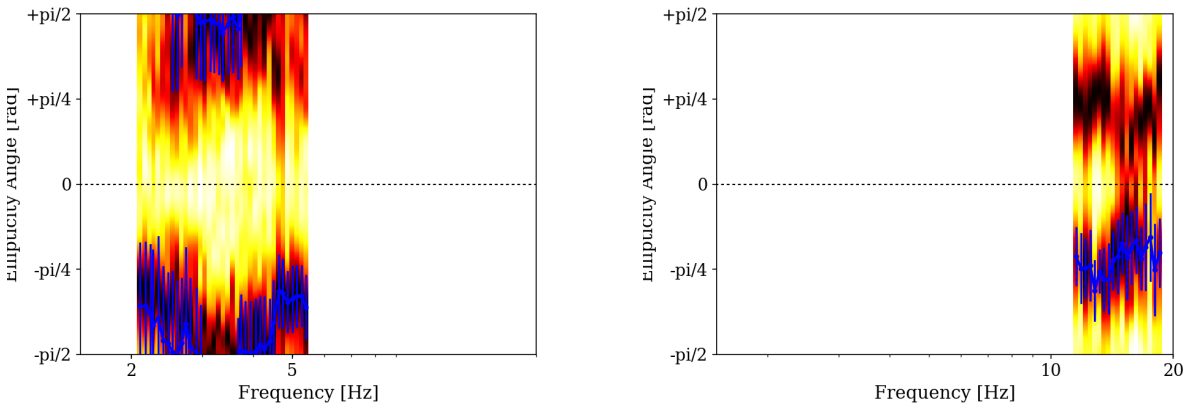

Figure 16: Ellipticity curve of the fundamental mode of Rayleigh waves with the WaveDec technique (Maranò et al., 2012).

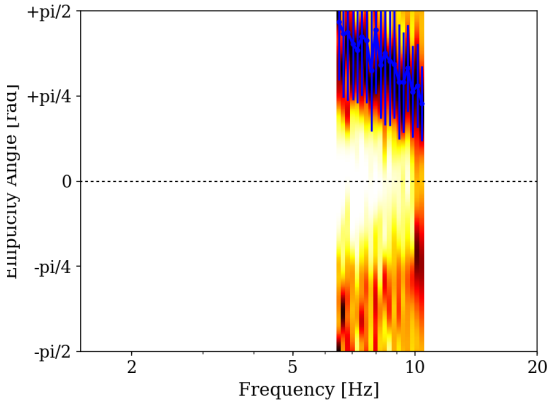

Figure 17: Ellipticity curve of the first higher mode of Rayleigh waves with the WaveDec technique (Maranò et al., 2012).

3.5 Interpretation

Fig. 18 gives an overview of the dispersion curves determined with the different methods. They provide broadband curves for the fundamental mode of Rayleigh waves (2.5 to 20 Hz) and of Love waves (2.5 to 18 Hz). The first higher mode of Rayleigh waves can also be reconstructed from 5 to 10 Hz. WaveDec results match well the HRFK observations except at low frequency, close to the array limit, and for Love waves around 9 Hz where they provide a continuous curve.
It is interesting to note that the second peak in the H/V curves at 3.5 Hz correspond to a point where fundamental Love and Rayleigh dispersion curves separate each other.

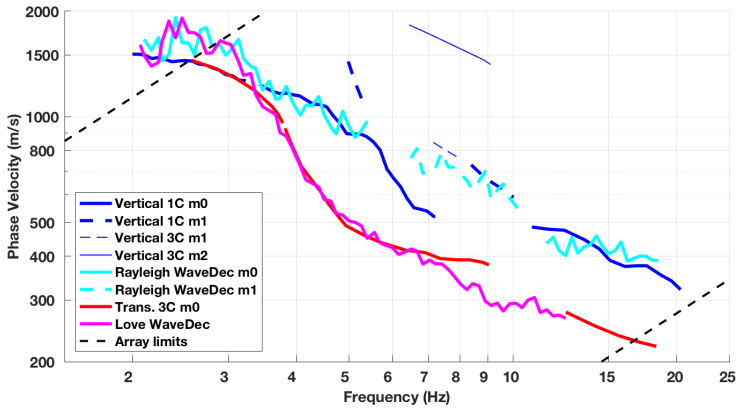

Figure 18: Picked dispersion curves from 1C and 3C HRFK analysis.

3.6 Data inversion

The inversion of the surface waves properties into 1D velocity profiles was performed using the Improved Neighborhood Algorithm (NA) (Wathelet, 2008) implemented in the Dinver software. In the inversion, 10000 starting models are used. 100 new cells are generated in the neighborhood of the 100 best cells (1 per cell) and 500 iterations of this process are performed. The process ends therefore with 60000 models explored.

3.6.1 Misfit function

The misfit function is based on the Rayleigh and Love wave fundamental mode dispersion curves, the Rayleigh first and second higher mode dispersion curves and ellipticity curve based on the TFA analysis code of V. Poggi, with a weight of 0.1. Since no singularity was found, we used the whole curve. Moreover, the fundamental resonance frequency at 0.7 Hz was used with a weight of 0.2 in order to constrain the results at depth. This means that we tried to retrieve the profiles until a great depth, not only the sediment part. All curves were resampled using 50 points between 0.4 and 20 Hz in log scale. No uncertainty was considered in the misfit function (all points with the same weight).

3.6.2 Parametrization of the model space

We assumed increasing velocity with depth (a test with a low velocity zone at 350 m depth, where the marls are found in the borehole, did not provide relevant results). The Poisson ratio was inverted in the range 0.2-0.4 (no water expected). The density was assumed to be 1800 kg/m^3 in the first 8 m, 2000 kg/m^3 in the sediments below this depth and 2500 kg/m^3 in the bedrock. Inversions with free layer depths as well as fixed layer depths were performed. 4 layers over a half space are enough to explain the targets (dispersion and ellipticity), but more layers are used to smooth the obtained results and better explore the parameter space. 5 independent runs of 5 different parametrization schemes (4 and 5 layers over a half space and 13, 14 and 16 layers with fixed depth) were performed, i.e. a total of 25 runs.

3.6.3 Results

Examples of retrieved ground profiles for the different strategies are presented in Fig. 19. The average misfit values for the best models of each inversion are not significantly different: 0.085 and 0.089 for the free layer depth strategy and 0.088, 0.089 and 0.096 for the fixed layer depth inversions. It can be noted that models with more layers have a slightly larger misfit here because it is more difficult to explore the parameter space. When comparing to the target curves (see Fig. 20 for an example with free layer depth, representative of the other computations) dispersion curves are well reproduced. The most noticeable deviation concerns Love waves around 5 Hz. The retrieved models produce a fundamental peak with too low values compared to the observations and the second peak has too high values compared to the observations. The retrieved value is 4 instead of 3.5 Hz. It should however be reminded that the site shows important lateral variations for this frequency peak, which makes the results satisfactory.
For further elaborations, the best models of these 25 runs were selected and used (see section 4.1).

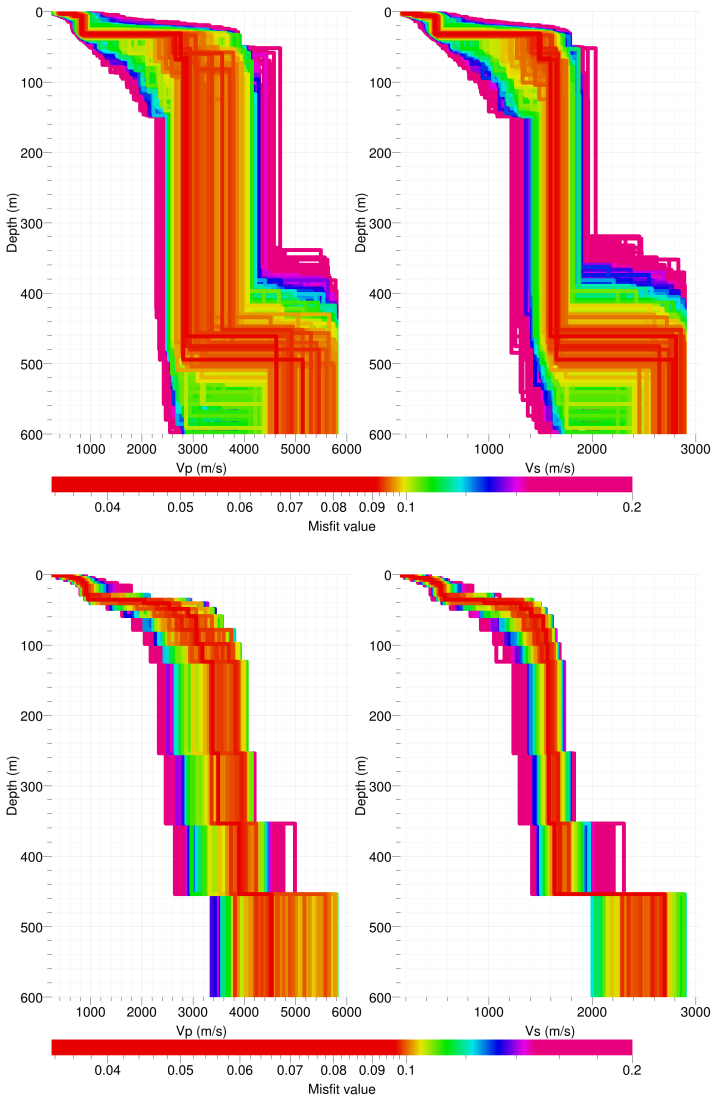

Figure 19: Inverted ground profiles at SLCF in terms of V_p and V_s using the free layer depth (6 layers - top) and the fixed layer depth (16 layers - bottom) strategies.

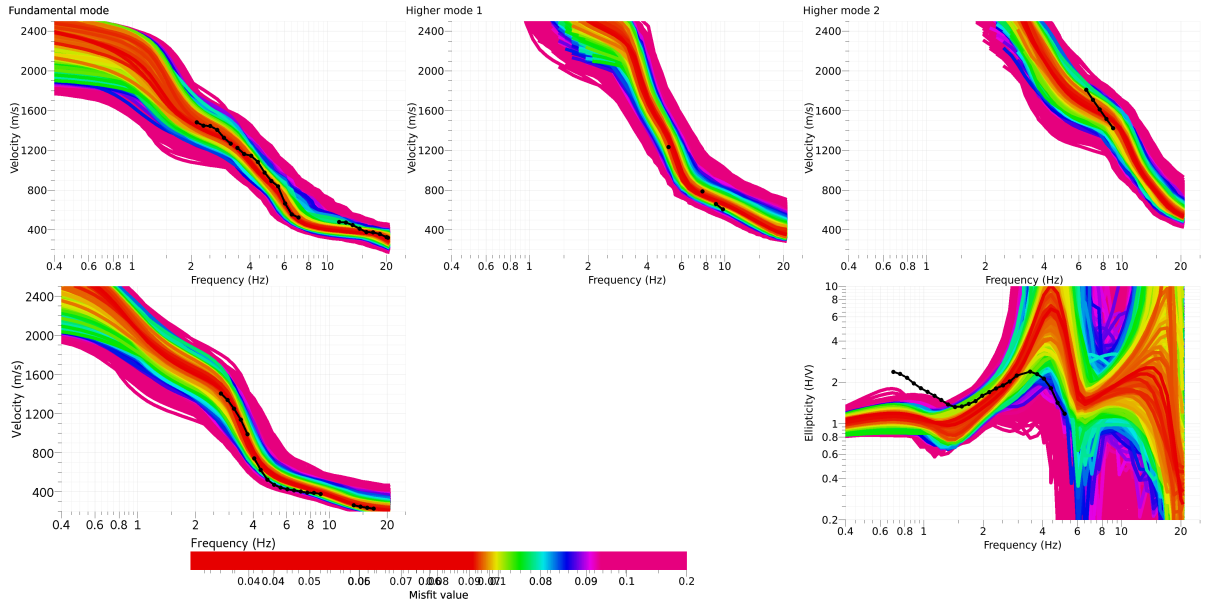

Figure 20: Comparison between inverted models and measured Rayleigh and Love waves (top row: Rayleigh dispersion fundamental, first and second higher modes; bottom row: Love fundamental dispersion curve left and Rayleigh waves ellipticity) at site SLCF for the 6 free layers inversion.

4 Interpretation of the velocity profiles

4.1 Velocity profiles

The profiles show low velocities from 180 m/s increasing to 520 m/s in the first 12 meters. The unconsolidated sediment layer goes down to 35 m depth with this constant velocity of 520 m. This layer is creating the 3.5 Hz resonance found in the H/V curves. The upper part of this layer is made of silts more or less clayey according to boreholes. In the borehole located 750 m SW of station SLCF, geotechnical tests on the silts showed that their stiffness increases with depth. At 15 m depth (deepest reached), they indicate NSPT values (per 30 cm) of about 40 that correspond to a Vs of about 350 m/s. It is improbable to interpret the 520 m/s layer as silts, most probably as morainic material. Below this depth, the velocity in the rock layers is gradually increasing from 1400 up to 1600 m/s at about 100 m depth, corresponding to conglomerates and massive Mesozoic limestone that cannot be distinguished. The inversion retrieves an interface at 450 m depth that creates the 0.7 Hz frequency peak. However, this result is highly speculative.

The distribution of the travel time average velocities at different depths was computed from the selected models. $V_{s,30}$ is found to be 405 m/s, corresponding to ground type B in the Eurocode 8 (CEN, 2004) and C in the SIA261 (SIA, 2014). Ground type E is not selected because of the depth of the unconsolidated sediments (35 m), while less than 20 m are required for type E.

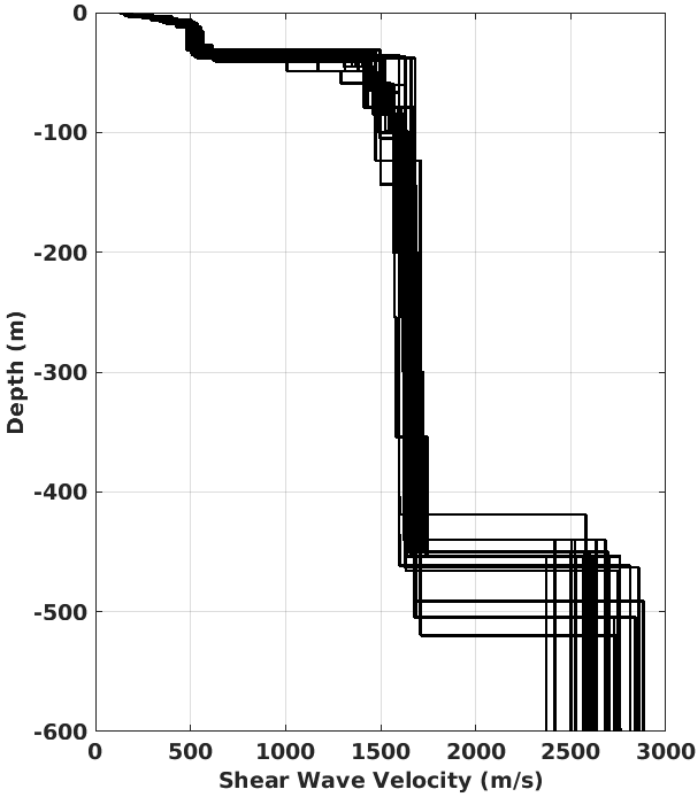

Figure 21: Shear-wave velocity profiles of the 25 selected models.

4.2 Quarter-wavelength representation

The quarter-wavelength velocity approach (Joyner et al., 1981) provides, for a given frequency, the average velocity at a depth corresponding to 1/4 of the wavelength of interest. It is useful to identify the frequency limits of the experimental data (minimum frequency in dispersion curves at 2 Hz and fundamental frequency of resonance at 0.7 Hz). The results using this proxy show that the dispersion curves constrain the profiles down to 90 m and the fundamental frequency to 500 m (Fig. 22). Moreover, the quarter wavelength impedance-contrast introduced by Poggi et al. (2012a) is also displayed in the figure. It corresponds to the ratio between two quarter-wavelength average velocities, respectively from the top and the bottom part of the velocity profile, at a given frequency (Poggi et al., 2012a). It shows a trough (inverse shows a peak) at the resonance frequency.

4.3 SH transfer function

The theoretical SH-wave transfer function for vertical propagation (Roesset, 1970) is computed from the selected profiles. It is corrected with respect to the Swiss Reference Rock model (Poggi et al., 2011) following Edwards et al. (2013). It shows a small peak at the fundamental frequency (0.7 Hz) and large peaks at about 4 and 10 Hz, reaching an amplification of 4.5 (Fig. 23). It is compared to the amplification function obtained by empirical spectral modelling (ESM) (Edwards et al., 2013; Michel et al., 2014, 2017). Although the empirical amplification for station SLCF is only based on few events so far, the theoretical SH transfer function of the retrieved profiles matches well this observed amplification function (Fig. 23).

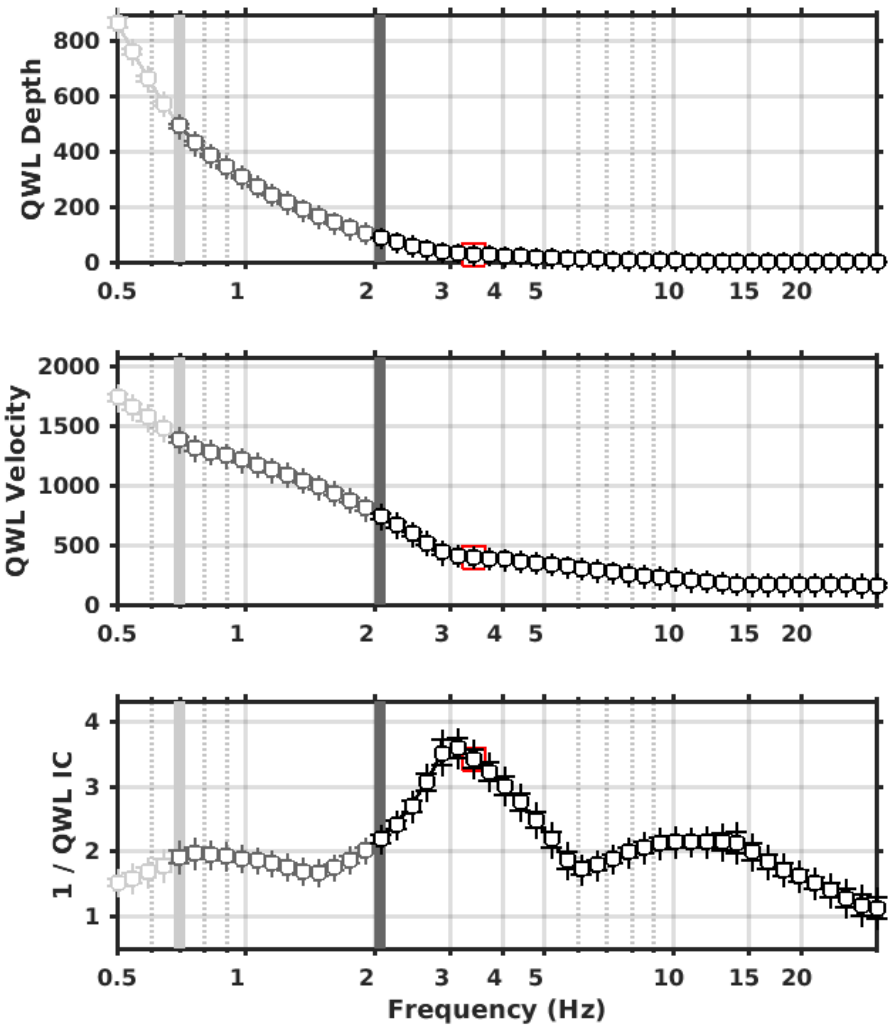

Figure 22: Quarter wavelength representation of the velocity profile for the selected velocity profiles (top: depth, center: velocity, bottom: inverse of the impedance contrast). The black curves are constrained by the dispersion curves, the light grey curves are not constrained by the data. The red square corresponds to V_{S30}.

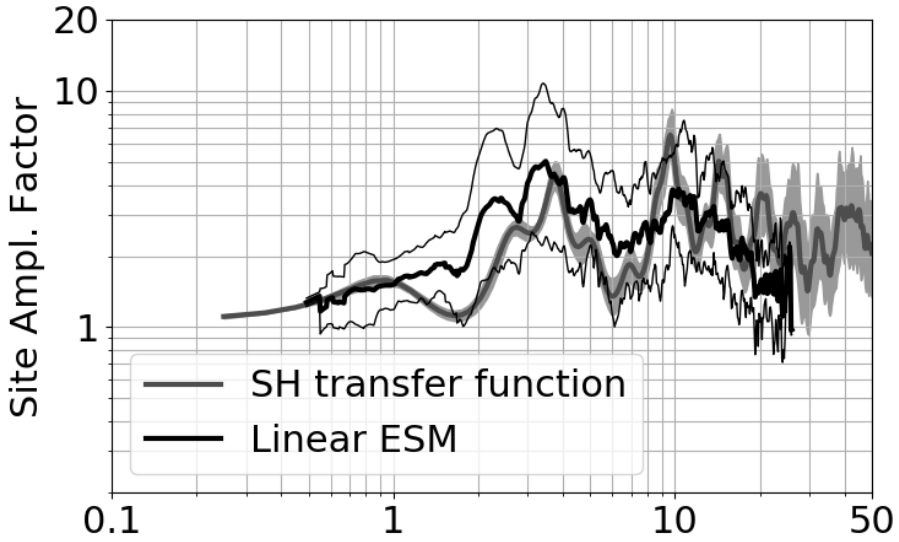

Figure 23: Comparison between the modeled SH transfer function for the selected velocity profiles and the empirical amplification (ESM) measured at station SLCF (with standard deviation).

5 Conclusions

The passive measurements presented in this study were successful in deriving a velocity model for the site SLCF. The profiles show 35 m of unconsolidated sediments with increasing velocities in the uppermost 12 m from 180 to 520 m/s. A clear contrast within the bedrock with velocity of about 1600 m/s is present at 35 m depth, creating the peak frequency at 3.5 Hz. We speculate about another velocity contrast at 450 m depth creating the fundamental frequency at 0.7 Hz.
$V_{s,30}$ is 405 m/s and the site corresponds to ground type B in the Eurocode 8 (CEN, 2004) and type C in the SIA261 (SIA, 2014). The theoretical 1D SH transfer function computed from the inverted profiles shows a large peak at the peak frequency at about 4 Hz reaching an amplification factor of 4.5. Though the sediments may be shallower in the city centre, the site is representative for the central part of the depression in La-Chaux-de-Fonds, while a large part of the city is sitting on rock.

Acknowledgements

The authors thank Simon Rouwendaal and Alejandro Duran for their help with the array measurements as well as Nadia Rognon from canton Neuchâtel who provided the borehole logs. An article written by Clément Grandjean on this measurement was published in the weekly magazine "Terre et Nature" on January 26th, 2017.

References

Burjánek, J., Gassner-Stamm, G., Poggi, V., Moore, J. R., and Fäh, D. (2010). Ambient vibration analysis of an unstable mountain slope. *Geophysical Journal International*, 180(2):820–828.

CEN (2004). *Eurocode 8: Design of structures for earthquake resistance - Part 1: General rules, seismic actions and rules for buildings*. European Committee for Standardization, en 1998-1: edition.

Edwards, B., Michel, C., Poggi, V., and Fäh, D. (2013). Determination of Site Amplification from Regional Seismicity : Application to the Swiss National Seismic Networks. *Seismological Research Letters*, 84(4).

Fäh, D., Kind, F., and Giardini, D. (2001). A theoretical investigation of average H/V ratios. *Geophysical Journal International*, 145(2):535–549.

Joyner, W. B., Warrick, R. E., and Fumal, T. E. (1981). The effect of Quaternary alluvium on strong ground motion in the Coyote Lake, California, earthquake of 1979. *Bulletin of the Seismological Society of America*, 71(4):1333–1349.

Maranò, S., Reller, C., Loeliger, H. A., and Fäh, D. (2012). Seismic waves estimation and wavefield decomposition: Application to ambient vibrations. *Geophysical Journal International*, 191(1):175–188.

Michel, C., Edwards, B., Poggi, V., Burjánek, J., Roten, D., Cauzzi, C., and Fäh, D. (2014). Assessment of Site Effects in Alpine Regions through Systematic Site Characterization of Seismic Stations. *Bulletin of the Seismological Society of America*, 104(6):2809–2826.

Michel, C., Fäh, D., Edwards, B., and Cauzzi, C. (2017). Site amplification at the city scale in Basel (Switzerland) from geophysical site characterization and spectral modelling of recorded earthquakes. *Physics and Chemistry of the Earth, Parts A/B/C*, 98:27–40.

Poggi, V., Edwards, B., and Fäh, D. (2011). Derivation of a Reference Shear-Wave Velocity Model from Empirical Site Amplification. *Bulletin of the Seismological Society of America*, 101(1):258–274.

Poggi, V., Edwards, B., and Fäh, D. (2012a). Characterizing the Vertical-to-Horizontal Ratio of Ground Motion at Soft-Sediment Sites. *Bulletin of the Seismological Society of America*, 102(6):2741–2756.

Poggi, V. and Fäh, D. (2010). Estimating Rayleigh wave particle motion from three-component array analysis of ambient vibrations. *Geophysical Journal International*, 180(1):251–267.

Poggi, V., Fäh, D., Burjánek, J., and Giardini, D. (2012b). The use of Rayleigh-wave ellipticity for site-specific hazard assessment and microzonation: application to the city of Lucerne, Switzerland. *Geophysical Journal International*, 188(3):1154–1172.

Roesset, J. (1970). Fundamentals of soil amplification. In Hansen, R. J., editor, *Seismic Design for Nuclear Power Plants*, pages 183–244. M.I.T. Press, Cambridge, Mass.

SIA (2014). *SIA 261 Einwirkungen auf Tragwerke*. Société suisse des ingénieurs et des architectes, Zurich, Switzerland.

Wathelet, M. (2008). An improved neighborhood algorithm: Parameter conditions and dynamic scaling. *Geophysical Research Letters*, 35(9):1–5.